Bull Earthquake Eng (2007) 5:325–345
DOI 10.1007/s10518-007-9034-5

ORIGINAL RESEARCH PAPER

Nonlinear numerical method for earthquake site response analysis II — case studies

Evelyne Foerster · Hormoz Modaressi

Received: 14 February 2006 / Accepted: 2 March 2007 / Published online: 30 June 2007

Abstract This paper presents two numerical case studies of medium and strong motion events, namely Loma-Prieta 1989 and Hyogoken-Nambu (Kobe) 1995. These simulations were performed using *CyberQuake* model. The cyclic elastoplastic constitutive model is fully detailed in the companion paper. Through these case studies, we demonstrate the importance of using appropriate constitutive modelling when the part played by nonlinear phenomena is preponderant. The need to account for 3D kinematics (i.e. the three components of the input motion), is also demonstrated, even though a 1D geometry is considered, as the plastic coupling existing between components of motion during the earthquake, strongly affects the seismic soil response.

Keywords Elastoplastic constitutive model · Parameter identification · Nonlinear earthquake simulation · Liquefaction

1 Introduction

The importance of local geological site conditions on the seismic ground response is now a well admitted fact. Indeed, the contrast prevailing for a given site, between the physical and mechanical properties of alluvial deposits and those of the underlying bedrock, produces what is called "site effects", that is an amplification/attenuation of the seismic motion observed at ground surface, as well as a modification of the frequency content, with respect to the reference rock motion. Recent strong earthquakes (Loma Prieta 1989, Rudbar-Manjil 1990, Northridge 1994, Hyogoken-Nambu/Kobe 1995) have demonstrated the crucial need for better local site characterizations, in order to predict their response more accurately in case of future earthquakes. Soil non-linearity, starting from very small strains, has been observed by several experimentalists (Seed and Idriss 1970; Hardin and Drnevich 1972; Kokusho 1980;

E. Foerster (✉)· H. Modaressi
Development Planning and Natural Risks Department, BRGM, BP 6009, 45060 Orleans Cedex 2, France
e-mail: e.foerster@brgm.fr

Vucetic and Dobry 1991), as well as by many field observations (Sugito and Kamada 1990; Chang et al. 1991; Beresnev et al. 1995; Elgamal et al. 1995; Mohammadioun 1997). It strongly affects the seismic motion of near-surface deposits, leading to: attenuation of the horizontal components and amplification of the vertical component of ground acceleration, shear wave velocity reduction, shift of the predominant frequency towards lower frequencies, irreversible settlements and lateral distortions. In-situ recordings (e.g. downhole seismic arrays) are essential to show the effects of both soil nonlinearity and soil failure (liquefaction) on the seismic ground response.

An appropriate model for soil deposits, such as the strain-hardening cyclic elastoplastic constitutive model detailed in the companion paper and used in the analyses presented in this paper, is thus required, in order to reproduce not only soil nonlinearity (variation of shear modulus and damping ratio in a wide range of distortion, namely from 10^{-6} to 10^{-2}), but also soil failure (pore-pressure build-up and mechanical degradation).

The simulations in this paper were performed using the nonlinear multi-kinematics transient dynamic model implemented in the computer program *CyberQuake*. This model is formulated on the basis of the effective stress principle and assumes the soil profile as a multi-layered drained or saturated deformable porous medium with homogeneous laterally infinite layers lying over a rigid or a deformable (elastic) bedrock (1D geometry). Soil layers below the water table are fully saturated and an undrained (one-phase) or partially drained (coupled two-phase) formulation is available. In this case, the bottom boundary is impervious (bedrock condition). In the one-phase case, total stresses are used in the governing equations and the pore-water pressure is derived from the constitutive parameters as: $p = -K\,\dot{\epsilon}_v^p$, with K, the bulk modulus and $\dot{\epsilon}_v^p$, the rate of volumetric plastic strain. In the coupled two-phase approach, both phases (water and solid) are explicitly considered and are assumed to be incompressible. The transient dynamic model is capable of predicting three-directional motions and to reproduce the previously mentioned complex features of soil behavior (nonlinearity and failure) under seismic loading.

In the next sections, we present the nonlinear simulations of the seismic soil response for two sites. The Port Island (Kobe, Japan) and Treasure Island (San Francisco, California) sites were chosen as: (1) they both have in place downhole seismic arrays; (2) large irrecoverable settlements, as well as evidence of liquefaction were indeed observed at these sites. Obviously, the nonlinearity associated to the elastoplasticity highlights the flaw of current 1D computations performed in practice, which assume body-wave decomposition hypothesis, i.e. SH-P/SV decomposition. This fact will be discussed, amongst others, in this paper.

2 Site response analysis at Treasure Island during the 1989 Loma-Prieta earthquake

2.1 Introduction

The Treasure Island site is a 162 ha reclaimed hydraulic fill built on a sand-Bay Mud shoal in the San Francisco Bay area (Fig. 1). The composition and consistency of the fill is mainly loose, fine to medium, silty sand, with occasional clayey zones. Liquefaction phenomena have been observed at this site after the 1989 Loma Prieta earthquake: observation of numerous sand boils, as well as large irrecoverable settlements and lateral spreading mainly in the North side of the site, essentially in the recent sub-

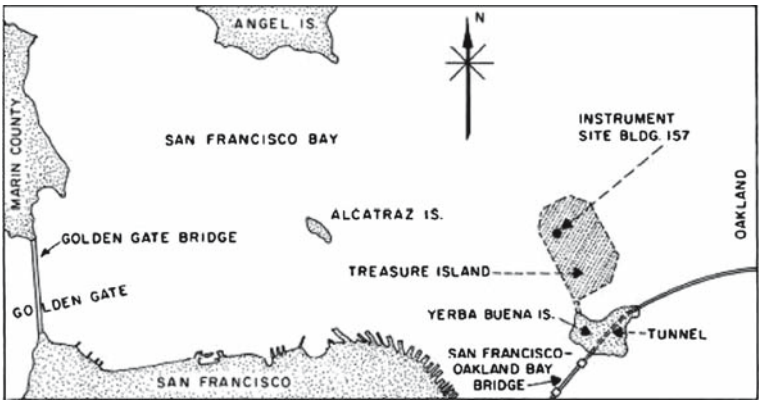

Fig. 1 Map of the San Francisco Bay (from CETS 1994)

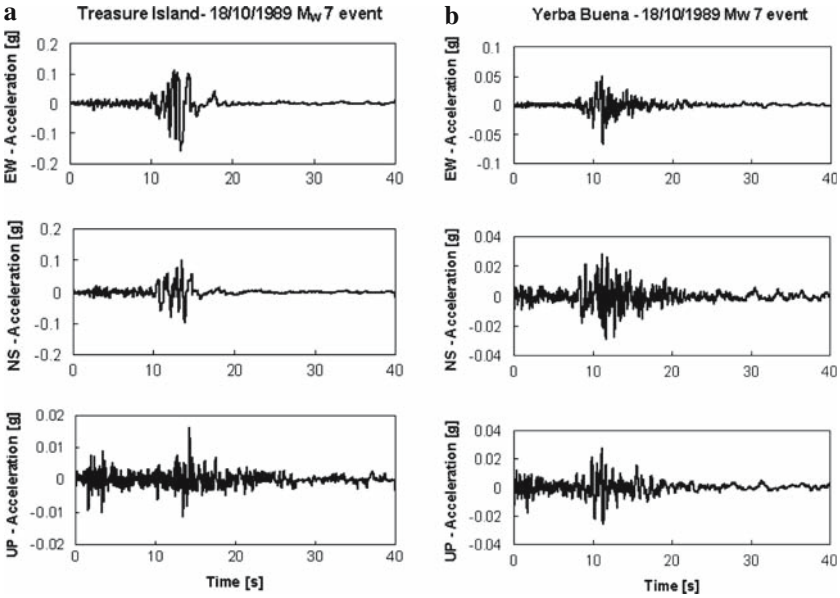

Fig. 2 Recorded accelerations at (**a**) Treasure Island site and (**b**) Yerba Buena rock outcrop

surface alluvial deposits. When analyzing the ground accelerations recorded at seismic fire station *CDMG code 58117* in the East–West (EW), North–South (NS) and vertical (UP) directions during the event, we note that these are considerably greater than those recorded by the nearby rock outcrop station (*CDMG code 58163*) on Yerba Buena Island (Fig. 2). The sudden drop of more than 0.15 g in the horizontal recorded accelerations, followed by low frequency oscillations, show that nonlinear site effects and soil failure occurred at the Treasure Island site (liquefaction after about 15 s of shaking).

Several site response studies using ground motion recordings obtained during the 1989 Loma Prieta earthquake, on fill material underlain by sediments at Treasure

Island and on rock at adjacent Yerba Buena Island, were made using the equivalent linear analysis (Seed et al. 1990) and the nonlinear analysis methods (Finn et al. 1993; Matasovic 1993).

In these studies, the computed surface response spectra were in general agreement with measured spectra. However, several of the analyses had some difficulty in capturing the recorded response in the short period/high frequency range. In this section, we present a similar site response analysis based on simulations of the free field seismic response, using the elastoplastic and equivalent linear approaches implemented in *CyberQuake* software. Computed and recorded ground accelerations, as well as response spectral acceleration are compared, considering either one component (horizontal) or three components of motion simultaneously.

2.2 Description of the soil profile

2.2.1 General features

After the M6.9 Loma Prieta earthquake of October 1989 and given the certainty of a future large motion event in the San Francisco Bay Area, it was decided to install a deep instrument array at the Treasure Island (TI) site in 1992, in order to assess possible ground motions but also behavior of soft soil sites (nonlinearity, etc.). There was no surface evidence of liquefaction at this site during the Loma Prieta event, but rather in the underlying hydraulic fill. Instrument installation was preceded by extensive site characterization. The instrument site is located at the island's fire station (Building 157) and is composed of 8 piezometers and 7 triaxial accelerometers situated at ground surface and various depths from the ground surface: at −7 m in the artificial sand fill; at −16 m in a silt-clayey mud layer (Young Bay Mud); at −31 m in a dense gray sand layer; at −44 m in a stiff clayey mud (Old Bay Mud); and finally at −104 m and −122 m, in the rock substratum (Fig. 3). The water table position was assumed to be located at 4 m depth. The physical characteristics used in our simulations for the soil profile (see Figs. 4, 5 and Table 1) were determined from the geophysical and geotechnical studies performed on the site (Gibbs et al. 1992; Hwang and Stokoe 1993; Pass 1994; Graizer et al. 2000). They are detailed in Table 2. A Poisson ratio of 0.3 was assumed for the materials of the site (Andrus et al. 1998).

2.2.2 Constitutive model parameters calibration

The constitutive model parameters presented in Table 3 were used in the nonlinear simulations. Details of the constitutive model and the related parameters can be found in the companion paper. In this analysis, most of the initial parameter values for clay layers (YBM and OBC) were derived by using the methodology proposed in the companion paper, with the available geotechnical data in Table 1. However, the remaining parameters, as well as the values given by the proposed methodology, were further calibrated by using the elastoplastic model simulator integrated in *CyberQuake*, in order to fit the G–γ and D–γ literature curves in Fig. 5. These calibrations were also performed for the layers with no available data.

As geotechnical data was missing for a number of layers, we have performed additional calibrations by computing the seismic response of the soil profile (Tables 2 and 3) for a recent weak event (17/08/1999, M_L 5), considering a nonlinear two-phase analysis and three components of motion. When comparing the EW and NS

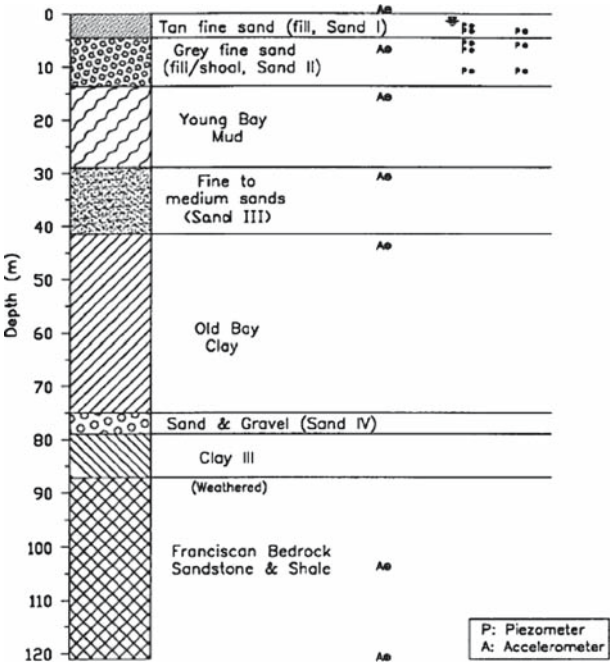

Fig. 3 Soil profile at the TI Fire Station (FS) site, showing piezometers (P) and accelerometers (A)

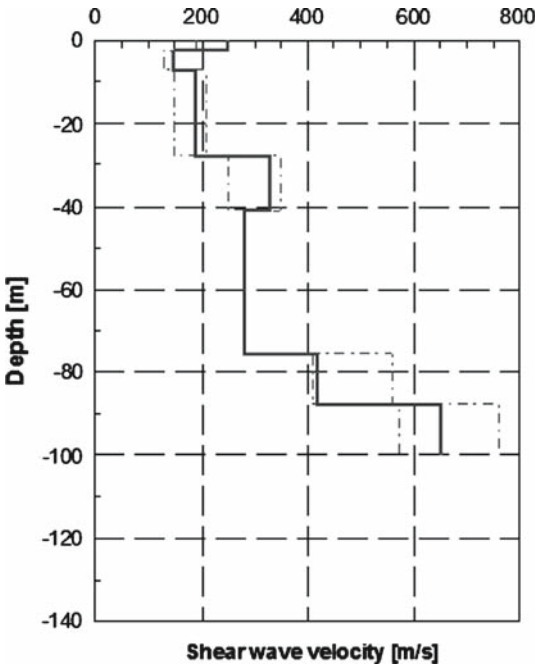

Fig. 4 S-wave velocity profile at Treasure Island site

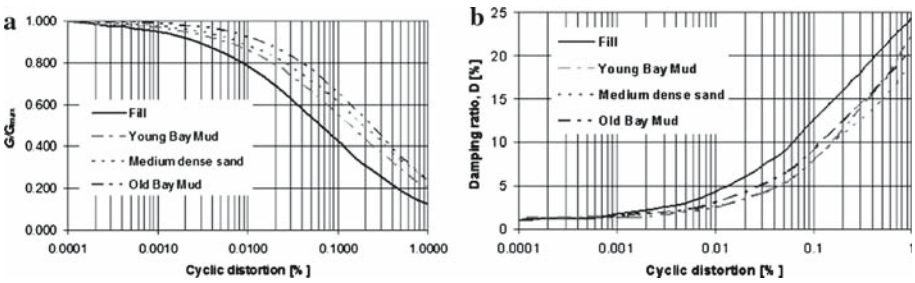

Fig. 5 (**a**) Shear modulus degradation and (**b**) damping ratio curves for TI site (after Hwang and Stokoe 1993)

Table 1 Clay properties summary for the TI FS site

	Young Bay Mud (YBM)	Old Bay Mud (OBC)
Plasticity index (%)	23	18
Clay fraction ($< 2\mu$m)(%)	33	18-35
Specific gravity (kN)	2.76	2.76
Void ratio, e	1.3	0.74
Wet unit weight (kg/m^3)	1762	1986
Over-consolidation ratio, OCR	1	2.8
Compression index, C_c	0.48	0.43
Undrained strength ratio (S_u/σ'_v)	0.26	?

Table 2 Soil profile features for the TI site model

Layer No.	Thick. (m)	Depth (m)	V_S (m/s)	V_P (m/s)	Density (kg/m^3)	Permeab. (m/s)	Material type
1	2.4	−2.4	250	468	2063	0	Gravelly sand fill (GS)
2	5.8	−8.2	135	253	2133	10^{-4}	Loose sand fill (LS)
3	5.5	−13.7	170	318	1842	10^{-6}	Silty loose sand fill (LSS)
4	15.2	−28.9	175	327	1794	10^{-8}	Young Bay Mud (YBM)
5	12.2	−41.1	315	589	1922	10^{-7}	Dense silty sands (DFS)
6	33.5	−74.6	265	496	1842	10^{-7}	Old Bay Mud (OBC)
7	13.7	−88.3	380	700	2082	10^{-9}	Gravelly sands / stiff clays (FGS)
Bedrock	–	–	650	1216	2082	–	Elastic

Water table at −4 m depth

Table 3 Parameters of the elastoplastic model (Treasure Island site)

Layer No.	Depth (m)	ϕ' (°)	ψ (°)	β	E_P	σ'_{c0}/σ'	b	γ^{ela}	γ^{hys}	γ^{mob}
1	−2.4	34	34	10	1000	10	0.8	10^{-7}	10^{-4}	10^{-3}
2	−4	30	27	40	100	1	0.1	10^{-7}	4.10^{-4}	5.10^{-3}
2	−8.2	30	27	40	60	0.3	0.1	10^{-7}	4.10^{-4}	5.10^{-3}
3	−13.7	34	27	40	140	0.2	0.2	10^{-7}	8.10^{-4}	10^{-3}
4	−16	25	25	10	120	1	1	10^{-9}	10^{-4}	10^{-3}
4	−28.9	25	25	10	150	2	1	10^{-9}	10^{-4}	10^{-3}
5	−31	34	30	40	120	3	0.5	10^{-7}	5.10^{-4}	10^{-3}
5	−41	34	30	40	200	3	0.2	10^{-7}	5.10^{-4}	10^{-3}
6	−74.6	25	25	10	200	3	1	10^{-9}	10^{-4}	10^{-3}
7	−88.3	25	25	10	250	3	1	10^{-9}	10^{-4}	10^{-2}

$n_r = 0.5$ and $\alpha_\psi = 1$ for all layers

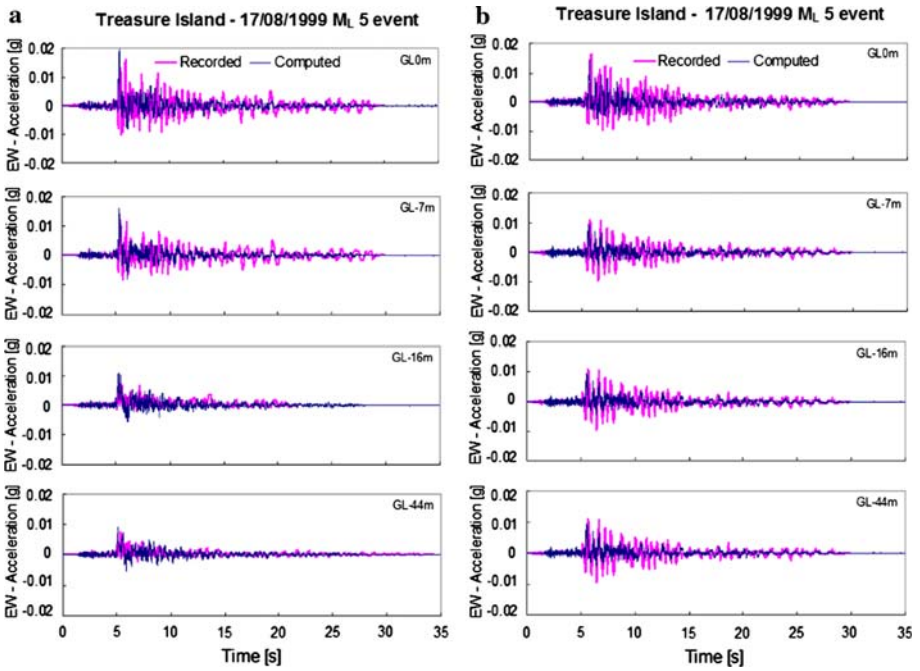

Fig. 6 Computed and measured (**a**) EW and (**b**) NS accelerations for the 17/08/1999 M_L 5 event

accelerations computed at various depths, as well as the related spectral accelerations on ground surface, with those recorded in the downhole seismic array during the event (Figs. 6, 7, respectively), we note that the computed shapes and frequency contents are in quite good agreement with the observations. However, such calibrations neglect possible incidence of any seismic event prior to the installation of the sensors.

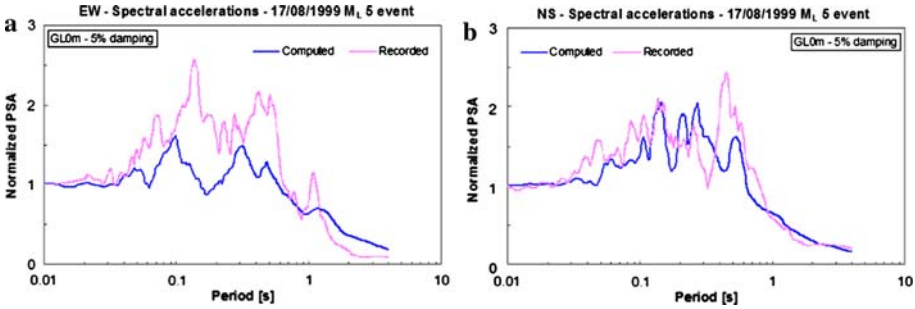

Fig. 7 Computed and recorded (**a**) EW and (**b**) NS normalized spectral accelerations for the 17/08/1999 M_L 5 event

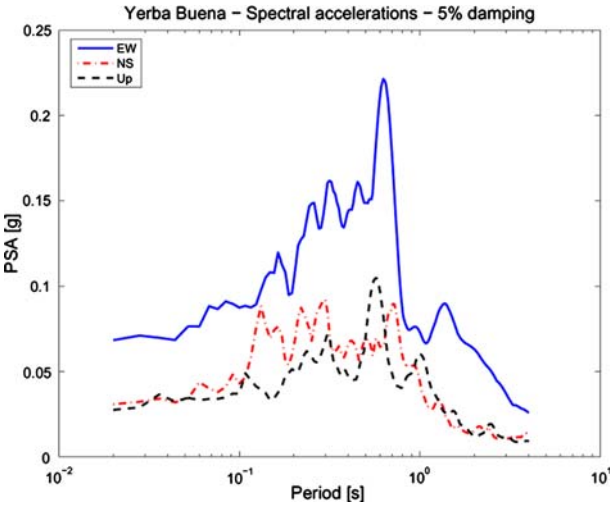

Fig. 8 Spectral accelerations for Yerba Buena input motion

2.3 Ground response analysis for the Loma Prieta 1989 event

2.3.1 Input motion

In this analysis, computations were performed, by considering the components of motion recorded at Yerba Buena (Fig. 8) as the input motion for the studied site. The observed peak ground acceleration (*PGA*) was equal to 0.22 g in the EW direction and the dominant period is of 0.63 s (Fig. 8). A maximum frequency of 15Hz was assumed in computations for this motion.

2.4 Numerical results and discussion

Three types of simulations were performed in this paper: one with the equivalent linear approach, and the two others, with the elastoplastic model (effective stress analyses), considering either a fully undrained (one-phase) or a partly drained (coupled two-phase) condition for layers underneath the water table. The G–γ and D–γ

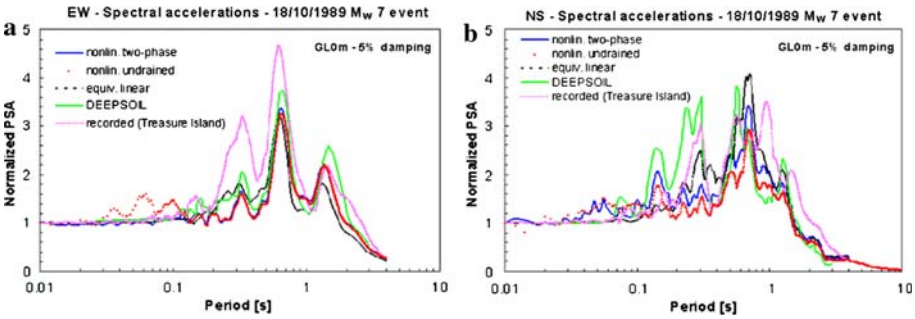

Fig. 9 Computed and recorded (**a**) EW and (**b**) NS normalized spectral accelerations for the 18/10/1989 M_W 7 event

curves required for the equivalent linear approach were computed with the elasto-plastic model.

Figure 9 shows the normalized spectral accelerations computed and recorded at ground surface, respectively in EW and NS directions, when considering three components of input motion. Curves obtained with the DEEPSOIL program are also presented (Hashash and Park 2002). In this latter approach, a new viscous damping formulation based on the full Rayleigh damping is introduced (time domain analysis), in order to improve nonlinear site response analysis at shorter periods. The proposed formulation allows the use of frequency dependent viscous damping and is more suited for wave propagation analysis in soil columns greater than 50 m thick.

The location of peak ground EW and NS accelerations, as well as the frequency content obtained with the nonlinear effective stress approaches are in good agreement with the observations, especially in the high period range. The equivalent linear approach underestimates all the observed peaks for the EW component and on the contrary, leads to a strong amplification of the NS acceleration, especially around 0.9 s. However, both effective stress analyses fail to reproduce the observed peaks around 0.3 s. This may be explained by the low coherence existing between the motions at Yerba Buena and Treasure Island in several frequency range, as mentioned by Finn et al. (1993). Computed and recorded ground accelerations versus. time for the non linear two-phase case are also presented in Fig. 10. A good agreement is found for the EW component, whereas NS and UP components tend to be underestimated. When comparing the variation of shear stresses versus shear strains at −11 m depth for the three approaches (Fig. 11), we see that liquefaction occurs for both directions in the undrained case, which is in accordance with the fact that the pore water pressure build-up is more important in this case (Fig. 12).

The comparison between the normalized NS acceleration response spectra obtained with three simultaneous components or only one (NS) component of motion in the nonlinear undrained case, is presented in Fig. 13. The spectral acceleration evaluated with the one component case is here in better agreement with the observed data, even at lower periods (e.g. around 0.3 s), which may be explained by the fact that plasticity is more mobilized in this case (see Fig. 14), leading to liquefaction at −11 m depth. In this particular case, we also note that plasticity seems to be more mobilized in the NS direction, when compared with the EW direction (Fig. 11). However, when the plasticity is mobilized to the same extent in both directions during the shaking event,

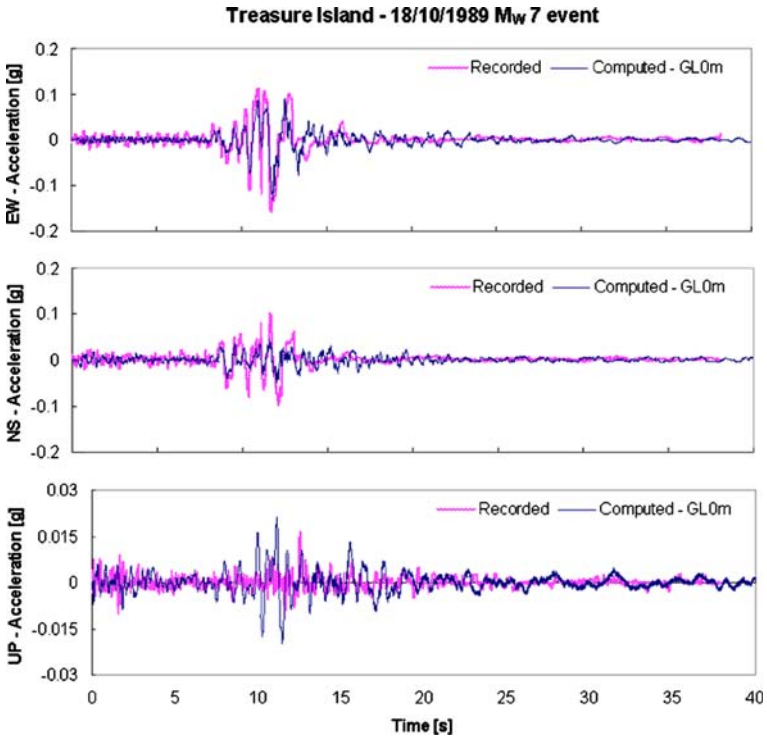

Fig. 10 Computed and recorded ground accelerations for the 18/10/1989 M_W 7 event (nonlinear two-phase simulation)

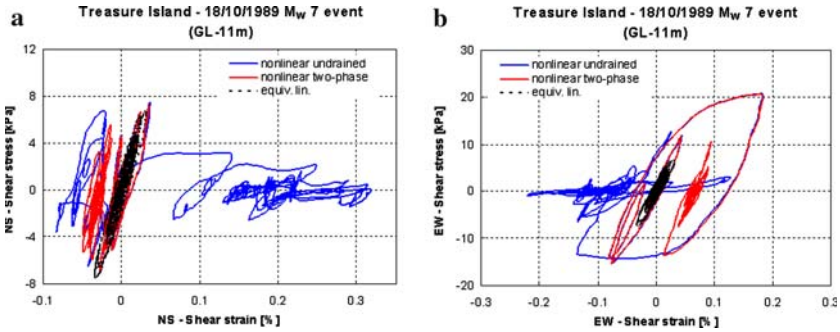

Fig. 11 Comparison of the computed (**a**) EW and (**b**) NS shear stresses versus shear strains variation at −11 m depth for the nonlinear and equivalent linear simulations (18/10/1989 M_W 7 event)

it is preferable to consider all components of input motion simultaneously in case of a nonlinear analysis, in order to obtain more realistic predictions. This has been shown for instance in a numerical site response analysis performed by Bernardie et al. (2006) on a site located in the Chang Hwa region during the 1999 Chi-Chi earthquake (Taiwan). This fact will be further discussed in the second case study.

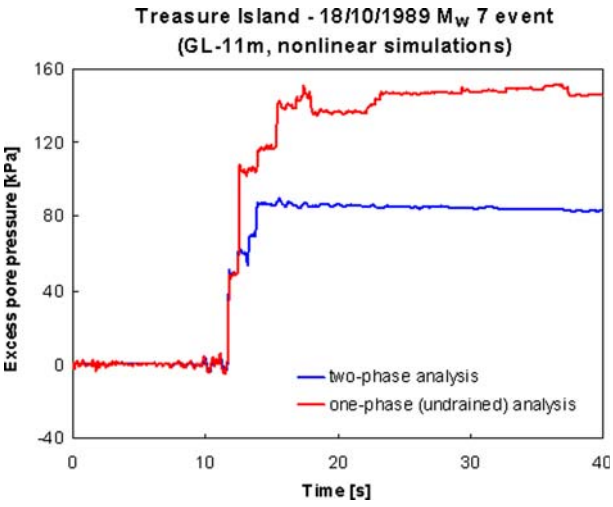

Fig. 12 Variation of the excess pore water pressures computed at −11 m depth for the undrained (one-phase) and coupled two-phase analyses (18/10/1989 M_W 7 event, nonlinear simulations)

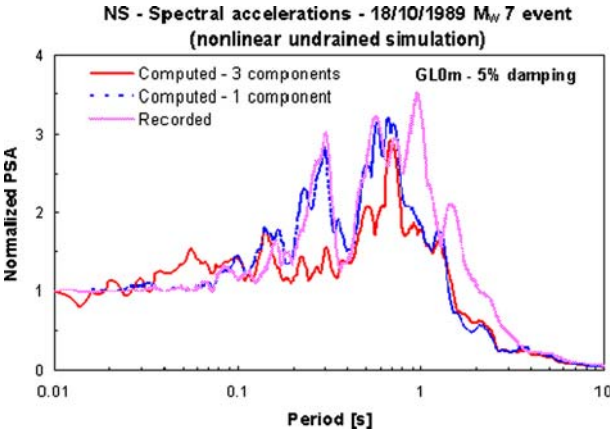

Fig. 13 Plastic coupling: comparison between computed (with one component and with three components of input motion) and recorded NS ground accelerations (undrained nonlinear simulations, 18/10/1989 M_W 7 event)

3 Site response analysis at Port Island during the 1995 Kobe earthquake

3.1 Introduction

By a close analysis of data recorded at Port Island vertical array during the 1995 Kobe earthquake, Mohammadioun (1997) has shown that nonlinearity in soil, evidenced by site liquefaction, resulted in an attenuation of the horizontal components of the acceleration recorded at ground surface and an amplification of the vertical one, compared to the bedrock motion. These observations are in good agreement with theoretical predictions made by Aubury and Modaressi (1992). In order to better

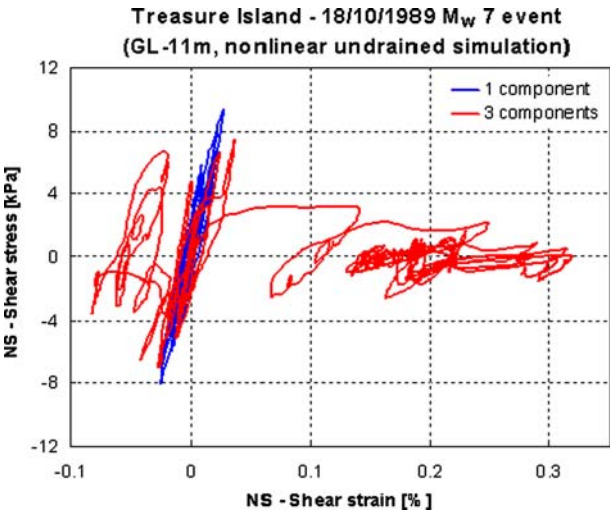

Fig. 14 Variation of the shear stresses versus shear strains computed at −11 m depth for one component and three component nonlinear undrained analyses (18/10/1989 M_W 7 event)

understand and then to be able to predict such effects, known as nonlinear site effects, it appeared necessary to implement downhole geotechnical arrays in the highly seismic zones. This type of arrays are at moment essentially located in California and in Japan. They provide the scientific community with geotechnical information relevant at the local scale, thanks to some receptors disposed at various depths. Moreover, they are also useful for separating local site effects from source or propagation effects.

In the next sections, we first recall the data available for this seismic response analysis of Port Island site during Kobe earthquake. The results obtained with the nonlinear model and the equivalent linear approach, are then compared with the field records provided at various depths down the vertical array existing on the site. In this strong motion event, nonlinear soil effects, such as site liquefaction, clearly appear on the recorded field data, as well as on the results from simulations.

3.2 Description of the soil profile

3.2.1 General features

In the Port Island downhole seismic array, accelerations were recorded using four triaxial accelerometers situated at various depths from the ground surface, respectively 0, 16, 32 and 83 m. The array was located on the north–west side of the reclaimed island very close to an improved ground area (Fig. 15). The array site itself consisted in 19 m of unimproved Masado (a decomposed granite fill), 8 m of alluvial clays, 34 m of sand with inter-layered clays, 18 m of diluvial clays and then sand under −79 m depth. The water table position was assumed to be located at 3 m depth. The physical characteristics used for the soil profile in our simulations are detailed in Table 4. Some data concerning the soil profile, i.e. shear wave velocities, or granulometric features,

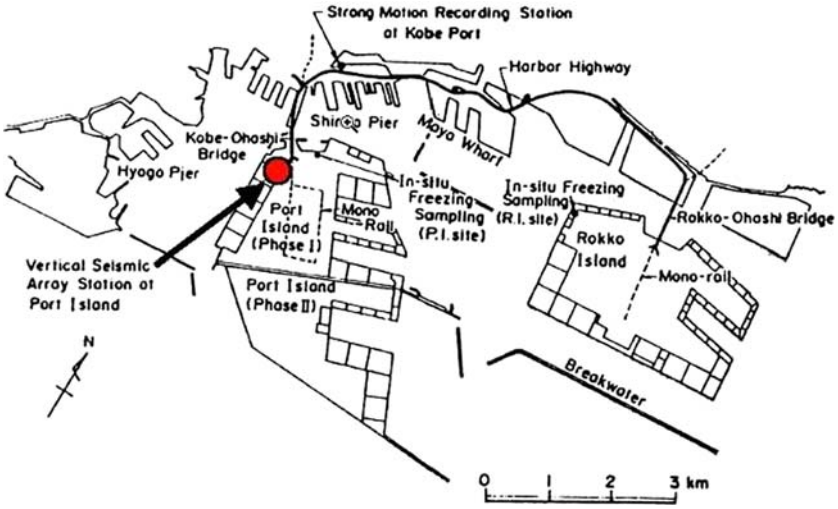

Fig. 15 Downhole seismic array location at Port Island site

Table 4 Soil profile features for the Port Island site model

Layer No.	Thick (m)	Depth (m)	V_S (m/s)	V_P (m/s)	Density (kg/m^3)	Permeab. (m/s)	Material type
1	2	−2	170	260	2000	5.10^{-4}	Granite fill (Masado)
2	3	−5	170	330	2000	5.10^{-4}	Granite fill (Masado)
3	7.6	−12.6	210	400	2200	2.10^{-4}	Granite fill (Masado)
4	6.4	−19	210	400	2200	2.10^{-4}	Gravelly sands
5	8	−27	180	350	1500	10^{-7}	Alluvial clays
6	5	−32	275	500	2000	10^{-4}	Diluvial sands
Bedrock	–	–	275	500	2000	–	Elastic

Water table at −3 m depth

were provided by the Port and Harbour Research Institute (1995) and were also found in the literature (Arulanandan and Li 2000).

3.2.2 Constitutive model parameters calibration

In this analysis, the methodology has essentially consisted in using the elastoplastic model simulator, in order to fit the experimental G–γ and D–γ curves. Predictions obtained with the constitutive model parameters presented in Table 5 are presented in Fig. 16.

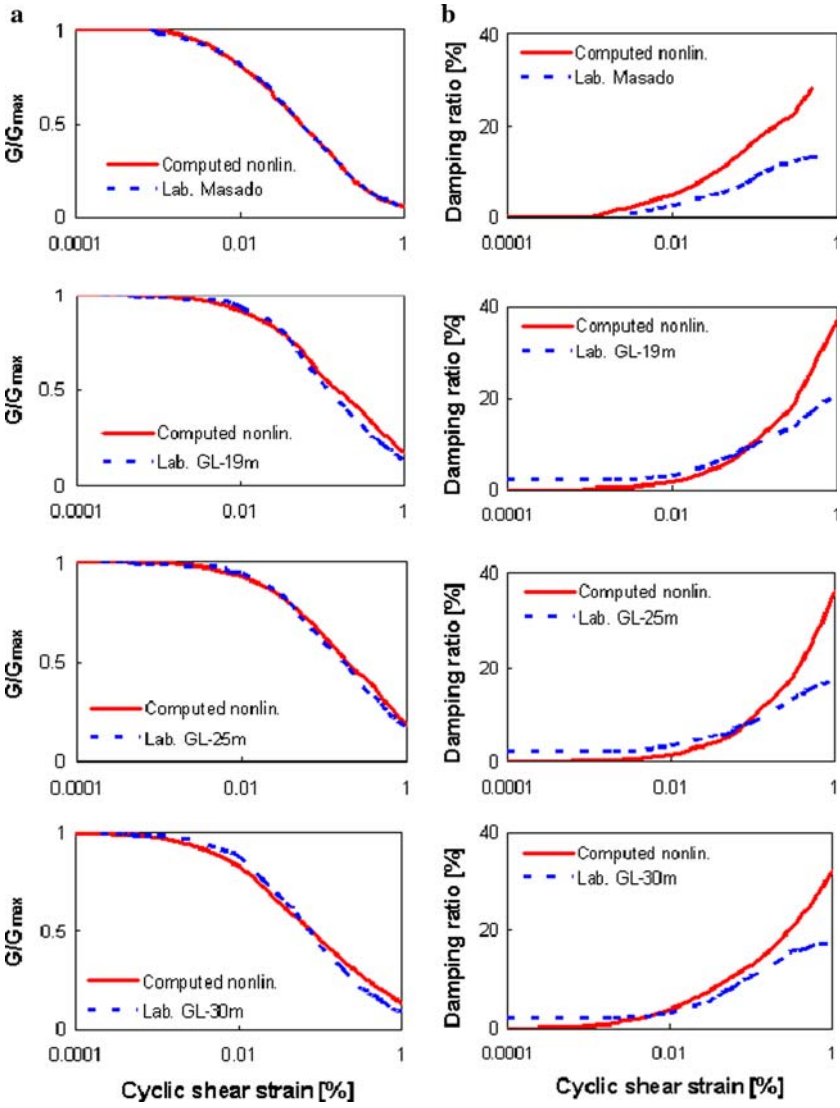

Fig. 16 Comparison of the shear modulus reduction and damping behavior curves obtained by laboratory tests (dashed line) and the elastoplastic model simulator (solid lines) for the Port Island site

3.3 Ground response analysis

3.3.1 Input motion

The North–South (NS) and East–West (EW) components of the input motion used for the simulations come from the incident wave at −32 m. This latter was obtained by an equivalent linear technique performed between −83 m and −32 m (Ishihara et al. 1998). A maximum frequency of 15Hz was assumed in computations for this motion.

Table 5 Parameters of the elastoplastic model (Port Island site)

Layer No.	Depth (m)	ϕ' (°)	ψ (°)	β	E_P	σ'_{c0}/σ'	b	γ^{ela}	γ^{hys}	γ^{mob}
1	−2	33	33	23	1500	10	0.5	10^{-6}	10^{-3}	10^{-1}
2	−3	33	33	23	800	2	0.5	10^{-6}	10^{-3}	10^{-1}
2	−5	33	33	23	300	2	0.5	10^{-6}	10^{-3}	10^{-1}
3	−12.6	30	30	11	50	1.5	0.2	10^{-8}	10^{-3}	10^{-1}
4	−16	33	33	15	100	2	0.24	10^{-8}	10^{-6}	10^{-1}
4	−19	33	33	15	100	2	0.24	10^{-8}	10^{-6}	10^{-1}
5	−27	22	22	9	150	1.1	1	10^{-10}	10^{-7}	10^{-3}
6	−32	35	32	11	110	5	0.3	10^{-8}	10^{-6}	10^{-1}

$n_r = 0.5$ and $\alpha_\psi = 1$ for all layers

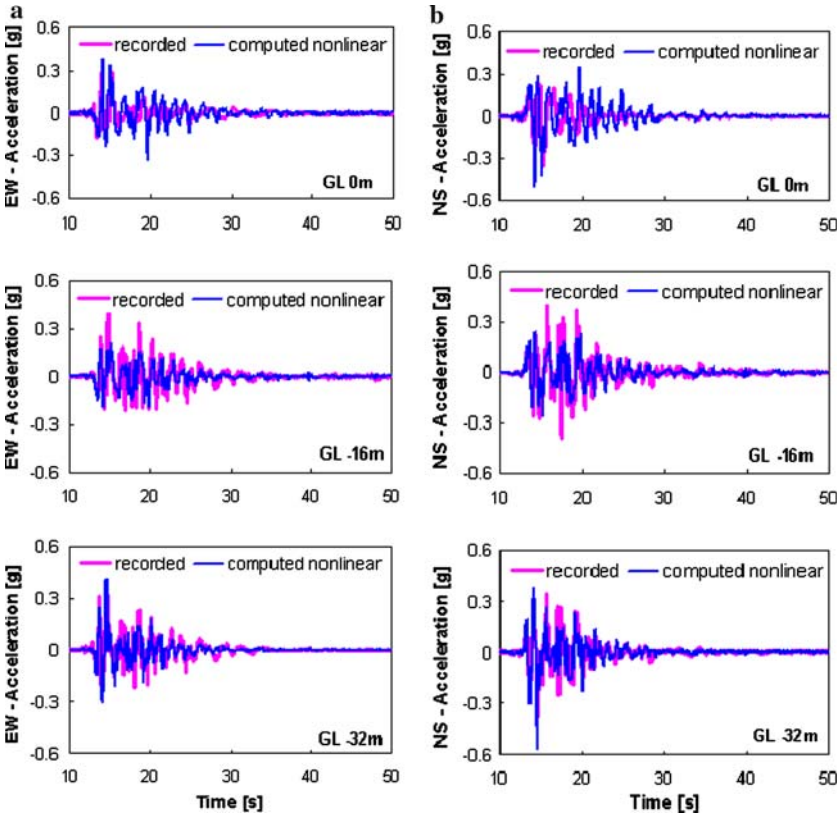

Fig. 17 Comparison between the computed and recorded (**a**) EW and (**b**) NS accelerations at various depths for the Port Island site (nonlinear undrained simulation)

3.4 Numerical results and discussion

Two simulations were performed: one with the elastoplastic model (effective stress analysis), considering a fully undrained condition for layers underneath the water table (one-phase analysis); the other with the equivalent linear approach. The G–γ

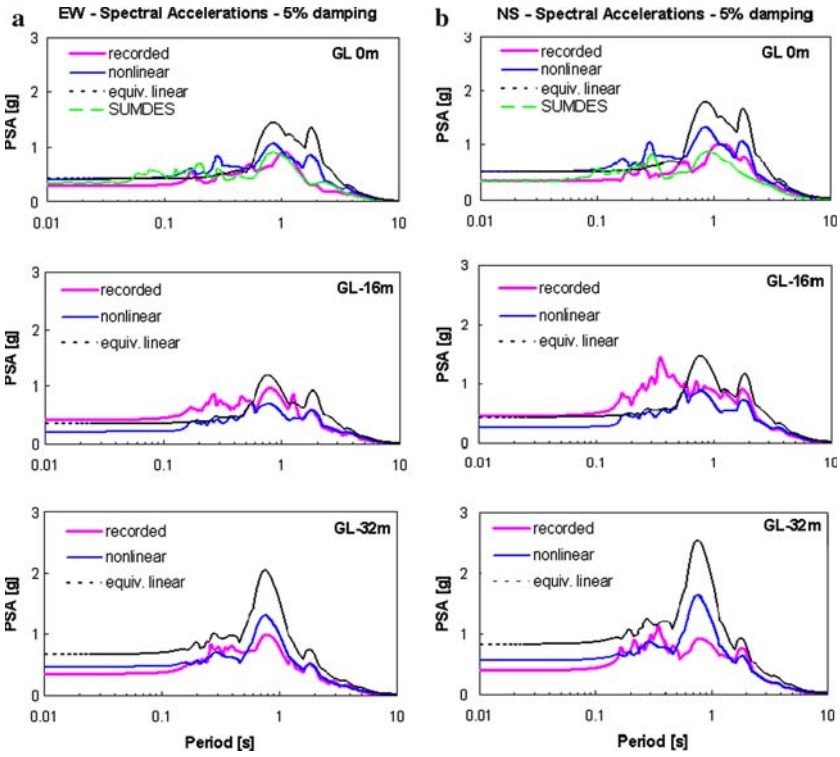

Fig. 18 Comparison between the computed and recorded (**a**) EW and (**b**) NS spectral accelerations at various depths for the Port Island site

and D–γ curves required for the equivalent linear approach were computed with the elastoplastic model (Fig. 16).

In the following, results obtained with the undrained simulation performed with *CyberQuake* will be referenced as "nonlinear".

The time history for the computed horizontal accelerations obtained at various depths for the nonlinear simulation are in good agreement with the recorded ones for both EW and NS directions, as shown in Fig. 17. Peak locations are well modelled, whereas a slight amplification of the amplitudes can be observed at ground surface around 20 s. Moreover, the computed accelerations at 16 m depth slightly underestimates the motion. The difference may be attributed to our insufficient knowledge of the geomechanical properties for the underlying layers.

Figure 18 shows the comparison between the spectral accelerations recorded and computed for the various simulations. Response spectra computed at ground surface with SUMDES are indicated for comparison (Arulanandan and Li 2000). At ground surface, all methods give response spectra with a little discrepancy in peak location. The amplitude of the response spectrum for the nonlinear approach is in good agreement with the observed one, whereas it is amplified with the equivalent linear method. In fact, as this technique represents a total stress analysis, it is unable to take into account the irrecoverable settlements and pore-water pressure build-up in the saturated soil. Thus, this approach may overestimate the intensity of the shaking.

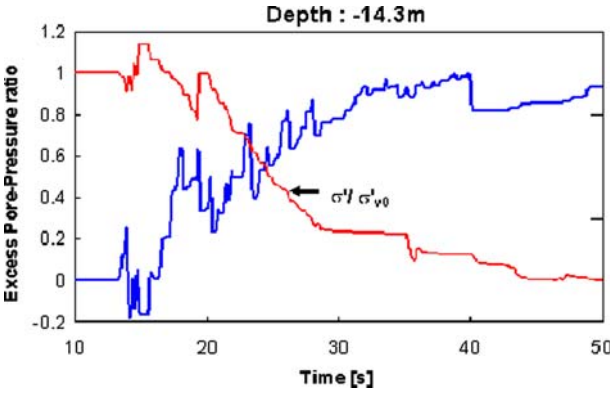

Fig. 19 Excess pore-pressure ratio computed at −14.3 m depth during the 1995 Kobe earthquake shaking (Port Island site)

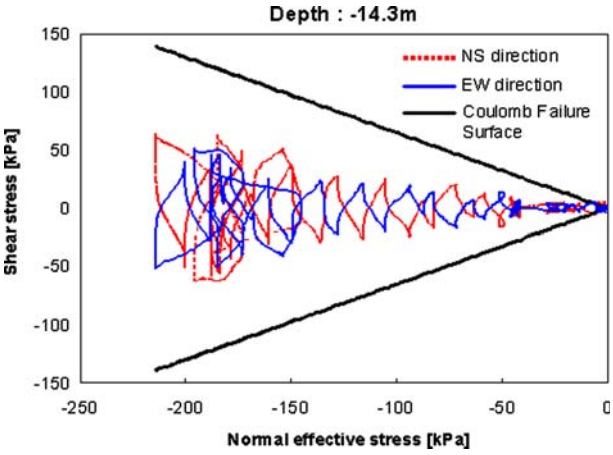

Fig. 20 Evolution of the shear stresses with respect to the effective normal stress, at −14.3 m depth during the 1995 Kobe earthquake shaking (Port Island site)

On the other hand, in the nonlinear undrained simulation, as the generated pore-pressure cannot dissipate during the shaking, the model is able to reproduce the aforementioned build-up and the annealing of the effective normal stress (Figs. 19, 20). The excess pore water pressure ratio variation with depth is shown on Fig. 21. As no field pore pressure measurements were reported for comparison with the computed pore water pressure during the seismic shaking, we have indicated some pressures evaluated with *CyberQuake* and with SUMDES (Arulanandan and Li 2000) at various depths. Plastic shear strain variation with depth computed at the end of the seismic shaking is shown in Fig. 22. The pore pressure ratio is a measure of liquefaction potential and the plastic shear strains are indicative of the possibly liquefied zones. In this case study, liquefaction was obtained between –8m and –16m (Figs. 19, 20), which is in good agreement with field observations and analyses made by various authors (Iwasaki and Tai 1995; Elgamal et al. 1996; Arulanandan and Li 2000). In Fig. 19, it may be seen that, around 20 s, the excess pore water pressure reduces

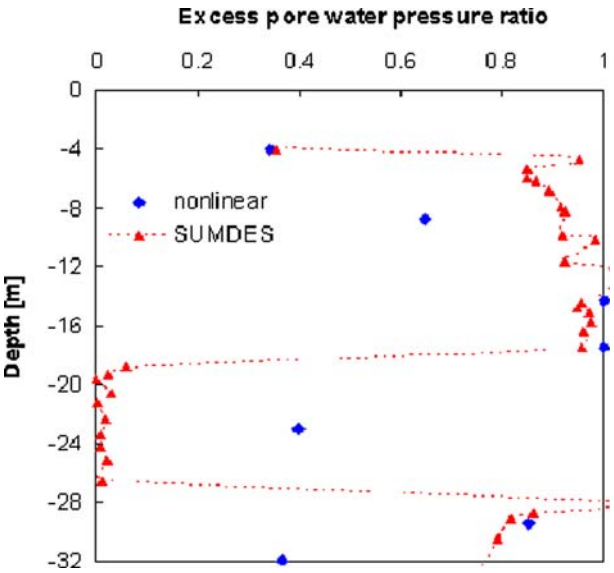

Fig. 21 Excess pore-pressure ratio variation with depth for the Port Island site

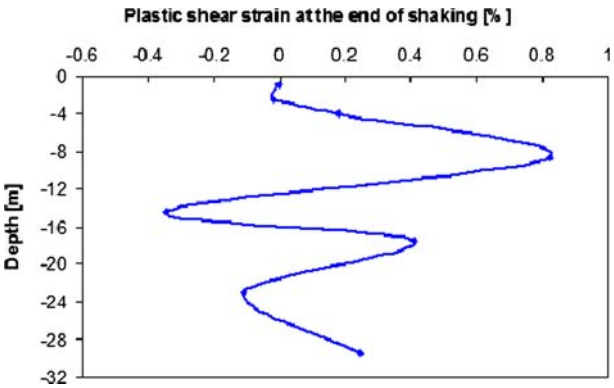

Fig. 22 Plastic shear strain variation with depth at the end of the seismic shaking for the Port Island site (nonlinear undrained simulation)

suddenly, due to soil dilatation at this depth. This strength recovery may explain the large peak observed at the same moment in the horizontal acceleration components as recorded at −16 m depth (Fig. 17).

The comparison between the normalized EW acceleration response spectra obtained with three simultaneous components or only one (EW) component of motion in the nonlinear undrained case, is presented in Fig. 23. The spectral acceleration evaluated with the three components case is here in better agreement with the observed data. Contrary to the Treasure Island case, the plasticity is here mobilized to the same extent in both directions (Fig. 24) during the shaking event, and thus, the coupling occurring at plasticity leads to more realistic predictions in this case.

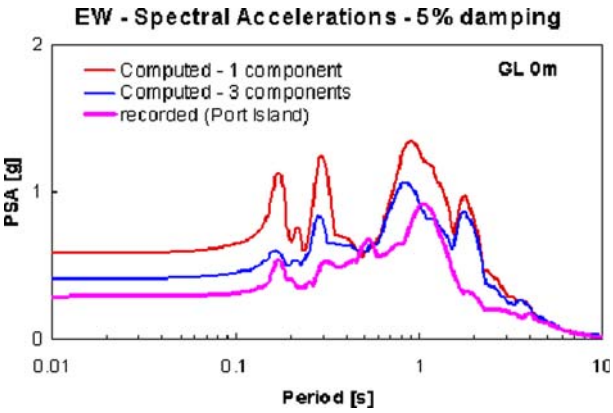

Fig. 23 Plastic coupling: comparison between computed (with one component and with three components of input motion) and recorded EW ground accelerations (undrained nonlinear simulations, Port Island site)

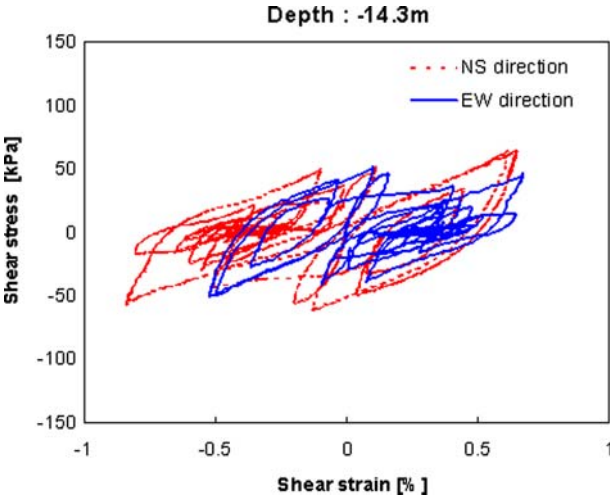

Fig. 24 Variation of shear stresses versus shear strains computed at −14.3 m depth when considering three components of motion (undrained nonlinear simulation, Port Island site)

4 Conclusions

In this paper, simulations were performed for two recent earthquakes (Loma Prieta 1989 and Kobe 1995), considered as strong motion events, using the the effective stress (cyclic elastoplastic constitutive modelling) and the equivalent linear approaches implemented in the *CyberQuake* program. These case studies demonstrate the capability of the non linear dynamic model to predict liquefaction potential in soft deposits under moderate or strong ground shaking. Indeed, the simulated ground responses, either with considering partly drained or fully undrained conditions for the layers underneath the water table, are generally in good agreement with the recorded accelerations.

For such strong events, we have shown that an analysis assuming one-dimensional geometry together with 3D kinematics (i.e. the three components of the input motion) and using an effective stress approach and an elastoplastic constitutive model, is able to reproduce the response of the studied sites generally with a better precision than the equivalent linear approach, which is based on 1D geometry and 1D kinematics. It is necessary to consider 3D kinematics when performing nonlinear computations, and not only one horizontal component as it is often performed in practice, in order to account for the coupling existing between components at plasticity and thus, to obtain more realistic predictions (Bernardie et al. 2006).

References

Andrus RD, Bay JA, Chung RM, Stokoe KH (1998) Liquefaction evaluation of densified sand at approach to pier 1 on Treasure Island, California, using SASW method. NIST Publication NISTIR 6230, 75–21

Arulanandan K, Li XS (2000) Numerical simulation of liquefaction-induced deformations. J Geotechn Geoenviron Eng 126(7):657–665

Aubry D, Modaressi H (1992) Seismic wave propagation in soils including non-linear and pore pressure effects. In: Davidovici V (ed) Recent advances in earthquake engineering and structural dynamics, Ouest Editions, pp 209–224

Beresnev IA, Wen K-L, Yeh YT (1995) Seismological evidence for nonlinear elastic ground behavior during large earthquakes. Soil Dynam Earthquake Eng 14(2):103–114

Bernardie S, Foerster E, Modaressi H (2006) Nonlinear site response simulations in Chang-Hwa region during the 1999 Chi-Chi earthquake, Taiwan. Soil Dynam Earthquake Eng 26(11):1038–1048

CETS (1994) Practical lessons from the Loma Prieta earthquake - report from a symposium sponsored by the geotechnical board and the board on natural disasters of the national research council. Commission on Engineering and Technical Systems, National Academy Press, Washington, DC

Chang CY, Power CM, Tang YK, Tang HT, Stepp JC (1991) Development of shear modulus reduction curves based on Lotung downhole data. In: 2nd international conference on recent advances in geotechnical earthquake engineering and soil dynamics. St Louis Rolla, Missouri. Eds. Prakash, pp 111–118

De Alba P, Benoit J, Pass DG, Carter J, Youd TL, Shakal A (1994) Deep instrumentation array at the Treasure Island Naval Station. The Loma Prieta, California, earthquake of October 17 1989 - strong ground motion. US Geol. Survey, Professional Paper 1551-A:155–168

Elgamal AW, Zeghal M, Tang HT, Stepp JC (1995) Lotung downhole array. I: evaluation of site dynamic properties. J Geotechn Eng ASCE 121(4):350–362

Elgamal AW, Zeghal M, Parra E (1996) Liquefaction of reclaimed island in Kobe, Japan. J Geotechn Eng ASCE 126(1):39–49

Finn WDL, Ventura CE, Wu G (1993) Analysis of ground motions at Treasure Island site during the 1989 Loma Prieta earthquake. Soil Dynam. Earthquake Eng 12(7):383–390

Gibbs JF, Fumal TE, Boore DM, Joyner WB (1992) Seismic velocities and geologic logs from borehole measurements at seven strong-motion stations that recorded the 1989 Loma Prieta earthquake. US Geological Survey Open-File Report 92–287

Graizer V, Shakal A, Hipley P (2000) Recent data recorded from downhole geotechnical arrays. In: SMIP 2000 Seminar on utilization of strong-motion data. California Division Mines and Geology, pp 23–38

Hardin BO, Drnevich VP (1972) Shear modulus and damping in soils : design equations and curves. J Soils Mechan Foundation Division ASCE 98(7):667–692

Hashash YMA, Park D (2002) Viscous damping formulation and high frequency motion propagation in non-linear site response analysis. Soil Dynam Earthquake Eng 22:611–624

Hwang SK, Stokoe KH (1993) Dynamic properties of undisturbed soil samples from Treasure Island, California. Civil Engineering Department Geotechnical Engineering Center, University of Texas at Austin,

Ishihara K, Kokusho T, Yasuda S, Goto Y, Yoshida N, Hatanaka M, Ito K (1998) Dynamic properties of Masado Fill in Kobe Port Island improved through soil compaction method – sumary of final

report. Technical report, Geotechnical Research Collaboration Committee on the Hanshin-Awaji Earthquake
Iwasaki Y, Tai M (1995) Strong motion records at Kobe Port Island. Special Issue of Soils and Foundations on Geotechnical Aspects of the January 17, 1995 Hyogoken-Nambu Earthquak SI(1):29–40
Kokusho T (1980) Cyclic triaxial test of dynamic soil properties for wide strain range. Soils Foundations 20(4):45–60
Matasovic N (1993) Seismic response of composite horizontally-layered soil deposits. PhD Thesis, University of California, Los Angeles
Modaressi A, Lopez-Caballero F (2001) Global methodology for soil behavior identification and its application to the study of site effects. In: 4th International conference on recent advances in geotechnical earthquake engineering and soil dynamics. San Diego, California. Eds. Prakash, p 1.08
Mohammadioun B (1997) Non-linear response of soils to horizontal and vertical bedrock earthquake motion. J Earthquake Eng 1(1):93–119
Pass DG (1994) Soil characterization of the deep accelerometer site at Treasure Island, San Francisco, California. MS Thesis in Civil Engineering, University of New Hampshire
Port and Harbour Research Institute (1995) Technical note No.813. Technical report, Ministry of Transport, Japan
Seed HB, Idriss IM (1970) Soil moduli and damping factors for dynamic response analyses. Report EERC-70-10, Earthquake Engineering Research Center
Seed RB, Dickenson SE, Riemer MF, Bray JD, Sitar N, Mitchell JK, Idriss IM, Kropp A, Harder LF, Jr, Power MS (1990) Preliminary Report on the Principal Geotechnical Aspects of the October 17, 1989 Loma Prieta Earthquake. Earthquake Engineering Research Center, Report No. UCB/EERC-90/05, University of California, Berkeley, 137 pp
Sugito M, Kamada H (1990) Non-linear soil amplification model with verification by vertical strong motion array records. Proc Japan Soc Civil Eng 531(I-34):51–63
Vucetic M, Dobry R (1991) Effect of soil plasticity on cyclic response. J Geotechn Eng ASCE 117(1):89–107